



Influence of the shot-peening intensity on the structure and near-surface mechanical properties of Ti₄₀Zr₁₀Cu₃₈Pd₁₂ bulk metallic glass

S. González, J. Fornell, E. Pellicer, S. Suriñach, M. D. Baró, A. L. Greer, F. J. Belzunce, and J. Sort

Citation: [Applied Physics Letters](#) **103**, 211907 (2013); doi: 10.1063/1.4833017

View online: <http://dx.doi.org/10.1063/1.4833017>

View Table of Contents: <http://scitation.aip.org/content/aip/journal/apl/103/21?ver=pdfcov>

Published by the [AIP Publishing](#)



Re-register for Table of Content Alerts

Create a profile.



Sign up today!



Influence of the shot-peening intensity on the structure and near-surface mechanical properties of $\text{Ti}_{40}\text{Zr}_{10}\text{Cu}_{38}\text{Pd}_{12}$ bulk metallic glass

S. González,^{1,a)} J. Fornell,¹ E. Pellicer,¹ S. Suriñach,¹ M. D. Baró,¹ A. L. Greer,^{2,3}
 F. J. Belzunce,⁴ and J. Sort^{5,a)}

¹Departament de Física, Facultat de Ciències, Universitat Autònoma de Barcelona, E-08193 Bellaterra, Spain

²Department of Materials Science and Metallurgy, University of Cambridge, 27 Charles Babbage Road, Cambridge CB3 0FS, United Kingdom

³WPI-Advanced Institute for Materials Research (WPI-AIMR), Tohoku University, Sendai 980-8577, Japan

⁴Instituto Universitario de Tecnología Industrial de Asturias IUTA, Universidad de Oviedo, E-33203 Gijón, Spain

⁵Institució Catalana de Recerca i Estudis Avançats (ICREA) and Departament de Física, Universitat Autònoma de Barcelona, E-08193 Bellaterra, Spain

(Received 29 August 2013; accepted 8 November 2013; published online 21 November 2013)

Shot-peening (SP) changes the near-surface structure and mechanical properties of a $\text{Ti}_{40}\text{Zr}_{10}\text{Cu}_{38}\text{Pd}_{12}$ bulk metallic glass. Near the surface, the hardness, Young's modulus, and elastic strain limit are all reduced. Measurements of the heat of relaxation show that an exceptionally high stored energy of cold work can be induced, implying a large increase in free volume. At the highest SP intensity there is partial nanocrystallization enabled by the increased free volume and not by the increase in temperature. © 2013 AIP Publishing LLC. [<http://dx.doi.org/10.1063/1.4833017>]

Bulk metallic glasses (BMGs) have attracted interest due to their high hardness and elastic limit, combined with easy flow when heated to above the glass-transition temperature, T_g , allowing thermoplastic molding and shaping with micro-scale precision.^{1–3} BMGs are of interest for sporting goods, medical and electronic devices, and defense and aerospace applications. However, BMGs exhibit poor room-temperature macroscopic plasticity compared to polycrystalline metals, due to formation and rapid propagation of shear bands.⁴ BMG plasticity can be improved by promoting the nucleation of shear bands and hindering their propagation by a wide variety of methods⁴ including surface treatments (e.g., shot peening (SP) or laser peening).⁵

In SP, the sample surface is repeatedly struck by beads at high velocity with impact energy sufficient to cause plastic deformation. For polycrystalline alloys, the technique is conventionally used to induce a compressive surface stress particularly effective in increasing fatigue resistance. SP also refines the microstructure.⁶ SP has been applied to BMGs to create multiple shear bands at the surface and to generate a compressive stress, enhancing the overall plasticity.⁵ SP also gives anisotropy in the surface layer and induces a less relaxed (damaged) glassy structure.^{7–9}

In a partially crystalline $\text{Zr}_{55}\text{Cu}_{30}\text{Al}_{10}\text{Ni}_5$ BMG, SP can induce either amorphization (or full crystallization) at higher (or lower) temperature.¹⁰ Crystallization was attributed to increased atomic mobility due to a large induced free volume V_f rather than to temperature rise. The role of V_f is studied further in the present work.

Structural changes observable in shot-peened surfaces are of interest as they aid understanding of changes (such as V_f creation and crystallization) seen in shear bands themselves. Thus, SP may be useful in fundamental studies of

plasticity mechanisms in BMGs, as well as in developing practical beneficial surface treatments.

Ingots, nominal composition $\text{Ti}_{40}\text{Zr}_{10}\text{Cu}_{38}\text{Pd}_{12}$ (at. %), were prepared by levitation melting a mixture of high-purity (99.9 wt. %) elements under argon. Rods (diameter 2.5 mm) were obtained by copper-mold casting. Cylindrical specimens were cut from the rod, and the top surface was ground, polished, and shot-peened. The SP intensity was assessed by the Almen method based on the curvature induced in standard (type A) steel strips.¹¹ Two treatments were applied: S1 (S2) with steel shot of diameter 0.4 (0.7) mm, air pressure of 1.5 (4.0) bar, peening time of 10 (20) s, giving an Almen intensity of 10 A (21 A). The SP was carried out at room temperature (i.e., 298 K) until attainment of 100% coverage.

The surface morphology after SP was observed with a scanning electron microscope (SEM) (Zeiss Merlin). Roughness was measured by profilometry with a confocal 3D optical surface metrology system LEICA DCM3D using blue light for high-resolution. The average line profile roughness (R_a) and surface area roughness (S_a) were obtained from four regions.

The as-cast and shot-peened samples were characterized by X-ray diffraction (XRD) (Philips X'Pert instrument, Cu-K α). Nanoindentation under load-control was performed using a UMIS instrument (Fischer-Cripps Laboratories) with a Berkovich pyramidal diamond tip applying a 10 mN maximum load. Thermal drift was below ± 0.05 nm s⁻¹. To study the effects of SP, the samples were cut perpendicular to the shot-peened surface, and nanoindentation tests were performed on the transverse section at different depths (distances from the surface). From the load-displacement ($P-h$) curves, the hardness (H), and reduced Young's modulus (E_r) were evaluated at the beginning of the unloading segments, using the method of Oliver and Pharr.^{12,13} Corrections for the contact area (calibrated using a fused-silica specimen), initial penetration depth, and instrumental compliance were

^{a)} Authors to whom correspondence should be addressed. Electronic addresses: sergio.gonzalez@uab.cat and jordi.sort@uab.cat

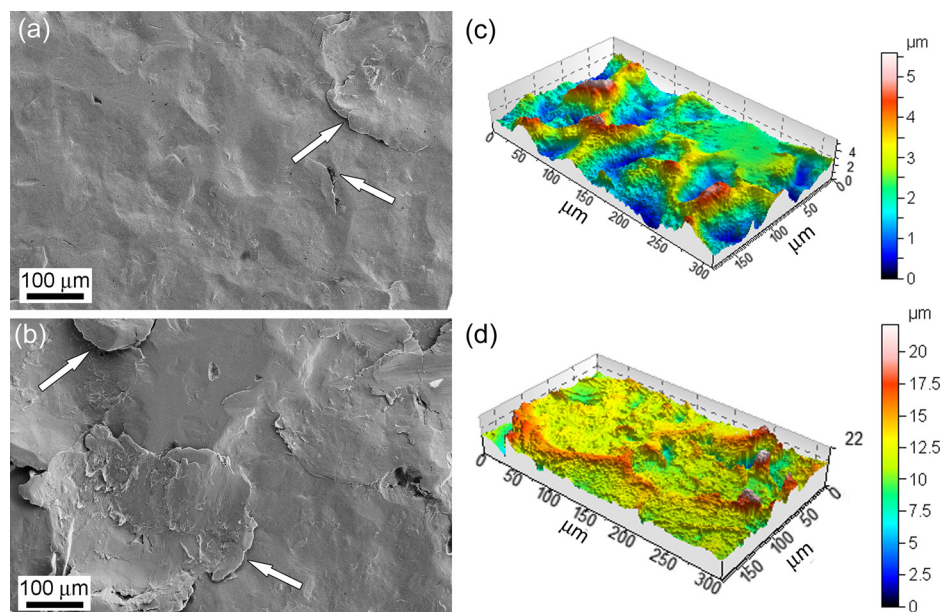


FIG. 1. SEM (a), (b) and profilometry ($310 \times 180 \mu\text{m}^2$) (c), (d) images of the surface of $\text{Ti}_{40}\text{Zr}_{10}\text{Cu}_{38}\text{Pd}_{12}$ BMG shot-peened under S_1 (a), (c) and S_2 (b), (d) conditions.

applied. The normalized plastic energy was evaluated as the ratio of plastic and total (plastic + elastic) energies during nanoindentation, $U_{\text{pl}}/U_{\text{tot}}$. Values of U_{pl} were calculated as the area between the loading and unloading nanoindentation curves while U_{tot} is the area between the loading curve and the displacement axis. The thermal stability of as-cast and shot-peened samples was investigated by differential scanning calorimetry (DSC), heating at 40 K/min in a Perkin-Elmer DSC7.

SEM and 3D profilometry images of shot-peened surfaces (Fig. 1) show that after S_1 treatment the surface is relatively smooth, with uniformly distributed shallow spherical craters; regions with detached material are scarce (white arrows). Under the harsher S_2 conditions, the surface is more heavily deformed, the perimeter of deep craters is well defined, and there is more detached material. The average roughness values were measured using profilometry: for S_2 $R_a = 0.99 \mu\text{m}$ and $S_a = 1.54 \mu\text{m}$, significantly greater than for S_1 with $R_a = 0.33 \mu\text{m}$ and $S_a = 0.63 \mu\text{m}$.

XRD from the S_1 sample surface shows a broad halo (Fig. 2(a)), indicating that the sample remains fully amorphous. The main diffraction halo becomes sharper after SP using S_2 conditions (Fig. 2(b)), suggesting that the sample

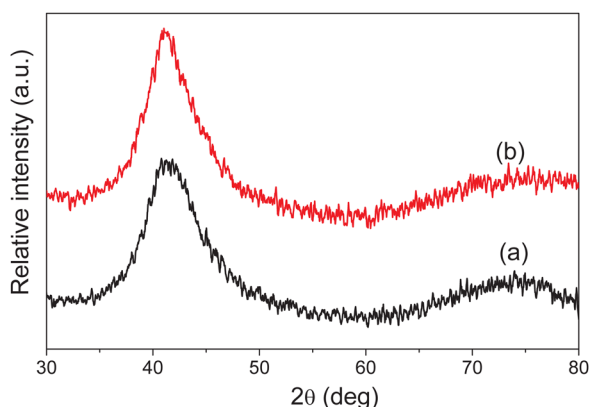


FIG. 2. XRD patterns from the surface of $\text{Ti}_{40}\text{Zr}_{10}\text{Cu}_{38}\text{Pd}_{12}$ BMG shot-peened under S_1 (a) and S_2 (b) conditions.

surface has become partly nanocrystalline (as observed after nanoindentation¹⁴ or severe plastic deformation¹⁵).

Shot-peened surfaces were analyzed by energy dispersive X-ray (EDX) spectroscopy. There was no evidence for iron or for oxides in sample S_1 , but oxide particles and iron (about 1 at. %) were detected for sample S_2 , particularly inside the deepest craters. Such contaminants may decrease the glass-forming ability¹ and catalyze the nucleation of nanocrystals.

Deformation causes softening in BMGs.^{3,16–18} Nanoindentation data (Fig. 3) show the profile of H , E_r , $U_{\text{pl}}/U_{\text{tot}}$, and σ_y/E as a function of distance from the surface for S_1 and S_2 samples. Both H and E_r progressively decrease, and the indentation plastic energy increases, within 50–100 μm from the shot-peened surface. The elastic strain limit, $\varepsilon_y = \sigma_y/E$, can be estimated using $H \approx 3\sigma_y$ and $E_r \approx E$. More realistic values of σ_y and ε_y (comparable to the as-cast sample, $\sigma_y \approx 2 \text{ GPa}$, and $\varepsilon_y \approx 0.02$)¹⁹ are obtained once an indentation size effect of around 35% for H and 20% for E is accounted for, in good agreement with the indentation size effect in other Ti-based BMGs.¹⁷ The results so obtained are plotted in Fig. 3(d) and indicate that SP lowers σ_y/E , consistent with the easier onset of plasticity expected in pre-deformed BMGs.

DSC curves were measured from thin slices cut at different distances from the peened surfaces (Fig. 4). No significant variations were observed in T_g ($\sim 686 \text{ K}$) or crystallization temperature ($T_x \approx 720 \text{ K}$) (Table I). The crystallization enthalpy is, however, smaller for slice S_2a ($H_{\text{crist}} = -6.26 \text{ kJ mol}^{-1}$) than for the other samples ($\sim -6.97 \text{ kJ mol}^{-1}$), suggesting that partial crystallization has taken place near the peened surface, consistent with the XRD results. However, three partially overlapped exothermic events are observed in all samples by DSC, indicating that no significant changes in the crystallization mode are induced, even after the most aggressive shot peening condition.

To interpret structure and property changes, it is useful to have a measure of the degree of SP-induced damage in the glassy structure. Damage can be characterized as increased

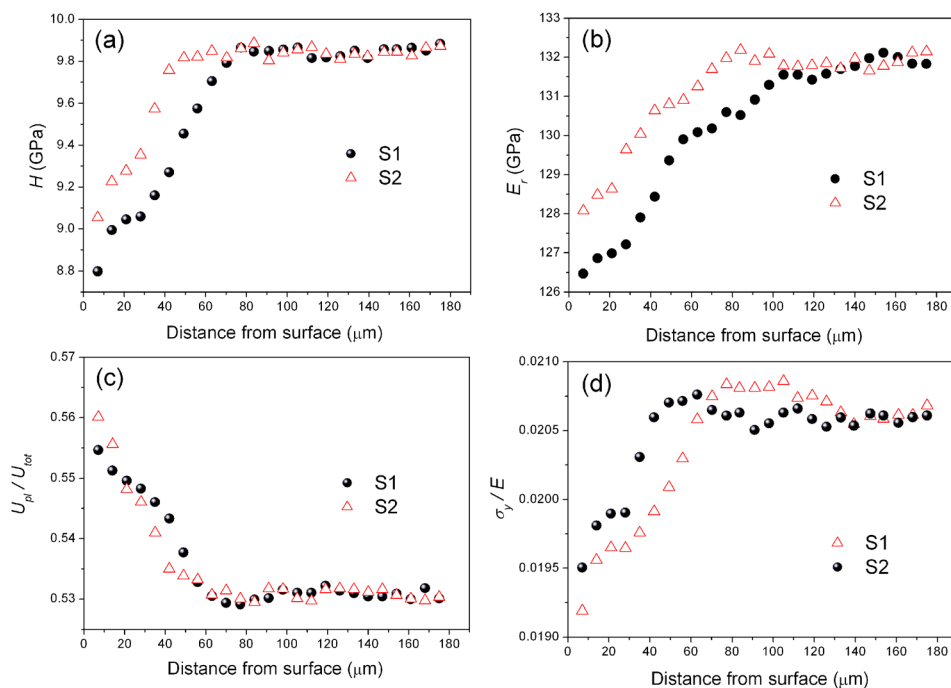


FIG. 3. Mechanical properties of $\text{Ti}_{40}\text{Zr}_{10}\text{Cu}_{38}\text{Pd}_{12}$ BMG as a function of the distance from the shot-peened surface: (a) hardness H , (b) reduced Young's modulus E_r , (c) normalized nanoindentation plastic energy U_{pl}/U_{tot} , and (d) elastic yield strain σ_y/E , estimated as described in the text.

free volume V_f and the enthalpy of a metallic glass can be linearly related to the V_f content.²⁰ Thus the stored energy of cold work, manifest as exothermic relaxation below T_g , is a

key parameter. The enthalpy of relaxation H_{relax} (Table I) increases dramatically after SP. This effect progressively decreases as the distance from the shot-peened surface is increased. This confirms earlier works^{8,9} that SP induces an increase in V_f . More V_f is generated in the S2 sample, despite the greater heating presumably induced during the more intense SP.

Increased V_f should lead to lower hardness, yet Fig. 3 shows that the deformation-induced decreases in H and E_r in S2 are smaller than for S1. While the surface oxide phases in sample S2 could contribute to the higher hardness, the most likely dominant cause is nanocrystallization, consistent with the XRD observations. The $\text{Ti}_{40}\text{Zr}_{10}\text{Cu}_{38}\text{Pd}_{12}$ BMG crystallizes to CuTi, CuTi₂, and CuZr intermetallic phases, giving increased H and E_r compared to the fully glassy structure.²¹

The observation of partial crystallization in the less relaxed surface layer of the S2 sample allows us to definitively exclude the possibility that the crystallization is induced by local heating. If local heating were responsible, the residual glassy phase would be more, not less relaxed than in the S1 sample. In previous work on BMGs, crystallization induced by SP was observed in only one case, when

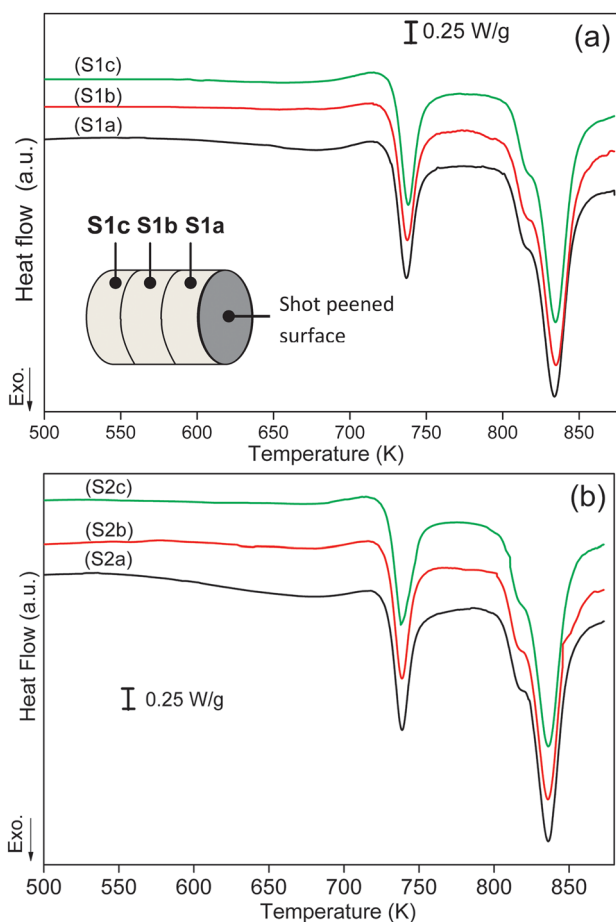


FIG. 4. DSC curves from thin slices cut at different depths from the shot-peened surfaces of S₁ and S₂ samples. Slices S1a, S1b, and S1c were cut at 450, 610, and 900 μm , and slices S2a, S2b, and S2c at 550, 756, and 916 μm , from the end surfaces of the BMG rods. For clarity, the curves are shifted along the y-axis.

TABLE I. The glass-transition temperature (T_g), crystallization temperature (T_x), relaxation enthalpy (H_{relax}), and crystallization enthalpy (H_{cryst}) for disks cut at different distances from the shot-peened surface (Fig. 4), for samples S1 and S2. H_{cryst} was measured as the area underneath the three observed crystallization peaks (Fig. 4).

Sample	T_g (± 2 K)	T_x (± 2 K)	H_{relax} (± 30 J mol ⁻¹)	$H_{cryst, \text{Sp peaks}}$ (± 60 J mol ⁻¹)
S1a	689	720	-360	-6970
S1b	693	720	-290	-6970
S1c	682	719	-290	-7040
S2a	689	718	-455	-6260
S2b	685	721	-290	-6910
S2c	686	717	-290	-7040

there were pre-existing crystals to seed the transformation and when the SP was at 77 K. It was inferred that the further crystallization took place, not during the SP itself, but during subsequent heating back to room temperature. In the present case there is no evidence for pre-existing crystals, and the crystallization occurs at the temperature of the SP itself. The magnitude of the stored energy of cold work is useful in understanding why crystallization can be induced in the present case.

The thickness of the top slices (450 μm for S1a; 550 μm for S2a) used for DSC is much larger than the material depth affected by the SP (<100 μm , Fig. 3). The increase in H_{relax} (i.e., stored energy of cold work) in slice S2a is $-455 - (-290) = -165 \text{ J mol}^{-1}$ when averaged over the slice. Given that only $\sim 20\%$ of the overall slice thickness is affected by SP, the increase in H_{relax} for the peened layer itself must be $\sim -825 \text{ J mol}^{-1}$. The decreased crystallization enthalpy in slice S2a (Table I) suggests a crystalline volume fraction of $(6970 - 6260)/6970 = 10\%$. Since only $\sim 20\%$ of the slice is affected by SP, this suggests a fraction as high as 50% in the peened layer. In that case, the increase in H_{relax} for the residual glassy phase in that layer is estimated to be $\sim -1650 \text{ J mol}^{-1}$ ($\approx 23\%$ of the crystallization enthalpy H_{cryst}).

For pre-annealed $\text{Pd}_{40}\text{Cu}_{30}\text{Ni}_{10}\text{P}_{20}$, the stored energy of cold work was at most -180 J mol^{-1} (-470 J mol^{-1}) from SP at 298 K (77 K).⁹ These values are comparable with the stored energies of up to -200 J mol^{-1} [Ref. 22] and -445 J mol^{-1} [Ref. 23] in cold-rolled ribbons of Pd- and Ni-based glasses. The value of $\sim -1650 \text{ J mol}^{-1}$, suggested in the present work, is much larger but still in the range of H_{relax} found in undeformed as-cast glasses. For example, for as-cast $\text{Pd}_{40}\text{Cu}_{30}\text{Ni}_{10}\text{P}_{20}$ BMG, $H_{\text{relax}} = -580 \text{ J mol}^{-1}$ [Ref. 9] while for melt-spun (i.e., rapidly quenched) ribbons of Fe-based glasses, the value of H_{relax} is as high as -5500 J mol^{-1} .²⁴

The greatly increased H_{relax} induced by the S2 treatment implies that SP induces a large increase in V_f . Yet the overall V_f is only comparable with, or less than that in, as-cast rapidly quenched glasses. SP-induced nanocrystallization may need to be interpreted not only in terms of the total V_f , but also in terms of its distribution. This distribution can be characterized from positron annihilation lifetime spectroscopy and from the thermal relaxation spectrum seen in DSC; deformation-induced changes in the distribution are reviewed in Ref. 9.

The large stored energy found in the S2 sample may be favored by the choice of steel shot instead of the glass beads used in previous works^{8,9} on SP of BMGs. In addition, inducing more damage because they are heavier, the steel shot must be more effective in extracting from the sample the heat generated during successive impacts.

To conclude, shot-peening the surface of $\text{Ti}_{40}\text{Zr}_{10}\text{Cu}_{38}\text{Pd}_{12}$ bulk metallic glass induces heavy plastic deformation that results in softening (reduction in hardness and in the elastic strain limit). The use of steel shot (rather than glass beads as in earlier work) gives a stored energy of

cold work in the peened glass estimated to be as high as -1650 J mol^{-1} , nearly four times the previous highest stored energy recorded in a metallic glass as a result of any mechanical treatment. The extreme deformation causes partial nanocrystallization of the surface. The coexistence of nanocrystallization and a highly unrelaxed glass means the underlying enhanced mobility that crystallization implies can be attributed to greatly increased free volume, and definitely not to heating. The onset of crystallization may be a key factor limiting the stored energy possible through cold work.

The authors thank the Servei de Microscòpia from UAB for the use of the confocal 3D optical Metrology System Leica DCM 3D microscope. Financial support from the MAT2011-27380-C02-01 research project from the Spanish MINECO and the 2009SGR-1292 from the Generalitat de Catalunya is acknowledged. J.F. and S.G. acknowledge the Ph.D. Fellowship and *Juan de la Cierva* contract from the Spanish Ministry of Science and Innovation, respectively. M.D.B. acknowledges funding support from an ICREA-Academia award, and A.L.G. acknowledges funding support from the Engineering and Physical Sciences Research Council (UK) and from the World Premier International Research Center Initiative (WPI), MEXT, Japan.

- ¹W. H. Wang, C. Dong, and C. H. Shek, *Mater. Sci. Eng. R* **44**, 45 (2004).
- ²M. F. Ashby and A. L. Greer, *Scr. Mater.* **54**, 321 (2006).
- ³C. A. Schuh, T. C. Hufnagel, and U. Ramamurty, *Acta Mater.* **55**, 4067 (2007).
- ⁴A. L. Greer, Y. Q. Cheng, and E. Ma, *Mater. Sci. Eng. R* **74**, 71 (2013).
- ⁵Y. Zhang, W. H. Wang, and A. L. Greer, *Nat. Mater.* **5**, 857 (2006).
- ⁶S. Bagheri and M. Guagliano, *Surf. Eng.* **25**, 3 (2009).
- ⁷F. O. Méar, G. Vaughan, A. R. Yavari, and A. L. Greer, *Philos. Mag. Lett.* **88**, 757 (2008).
- ⁸F. O. Méar, B. Lenk, Y. Zhang, and A. L. Greer, *Scr. Mater.* **59**, 1243 (2008).
- ⁹A. Concustell, F. O. Méar, S. Suriñach, M. D. Baró, and A. L. Greer, *Philos. Mag. Lett.* **89**, 831 (2009).
- ¹⁰F. O. Méar, B. Doisneau, A. R. Yavari, and A. L. Greer, *J. Alloys Compd.* **483**, 256 (2009).
- ¹¹M. Guagliano, *J. Mater. Proc. Technol.* **110**, 277 (2001).
- ¹²W. C. Oliver and G. M. Pharr, *J. Mater. Res.* **7**, 1564 (1992).
- ¹³A. C. Fischer-Cripps, *Nanoindentation* (Springer-Verlag, Inc., New York, 2002).
- ¹⁴J. Fornell, E. Rossinyol, S. Suriñach, M. D. Baró, and J. Sort, *Scr. Mater.* **62**, 13 (2010).
- ¹⁵P. Henits, Á. Révész, A. P. Zhilyaev, and Zs. Kovács, *J. Alloys Compd.* **461**, 195 (2008).
- ¹⁶N. Van Steenberge, J. Sort, A. Concustell, J. Das, S. Scudino, S. Suriñach, J. Eckert, and M. D. Baró, *Scr. Mater.* **56**, 605 (2007).
- ¹⁷J. Fornell, A. Concustell, S. Suriñach, W. H. Li, N. Cuadrado, A. Gebert, M. D. Baró, and J. Sort, *Int. J. Plast.* **25**, 1540 (2009).
- ¹⁸A. Concustell, J. Sort, G. Alcalá, S. Mato, A. Gebert, J. Eckert, and M. D. Baró, *J. Mater. Res.* **20**, 2719 (2005).
- ¹⁹J. Fornell, S. González, E. Pellicer, N. Van Steenberge, P. Pérez, S. Suriñach, M. D. Baró, and J. Sort, *J. Alloys Compd.* **536**, S74 (2012).
- ²⁰A. van den Beukel and J. Sietsma, *Acta Metall. Mater.* **38**, 383 (1990).
- ²¹J. Fornell, N. Van Steenberge, A. Varea, E. Rossinyol, E. Pellicer, S. Suriñach, M. D. Baró, and J. Sort, *J. Mech. Behav. Biomed. Mater.* **4**, 1709 (2011).
- ²²H. S. Chen, *Appl. Phys. Lett.* **29**, 328 (1976).
- ²³B. Jessen and E. Woldt, *Thermochim. Acta* **151**, 179 (1989).
- ²⁴L. Battezzati, G. Riontino, M. Baricco, A. Lucci, and F. Marino, *J. Non-Cryst. Solids* **61–62**, 877 (1984).